PLACEMENT OF VIRTUAL INERTIA IN ISLANDED DISTRIBUTION NETWORKS WITH HIGH PENETRATION OF INVERTER-BASED RESOURCES

Fadi Kelada, Jérôme Buire, Nouredine Hadjsaid

PLACEMENT OF VIRTUAL INERTIA IN ISLANDED DISTRIBUTION NETWORKS WITH HIGH PENETRATION OF INVERTER-BASED RESOURCES

Fadi KELADA[1], Jérôme BUIRE[1], Nouredine HADJSAID[1,2]
[1] Univ. Grenoble Alpes, CNRS, Grenoble INP*, G2ELab, F-38000 Grenoble, France
* Institute of Engineering Univ. Grenoble Alpes
[2] Nanyang Technological University, Singapore 639798, Singapore
E-mail: {fadi.kelada, jerome.buire, nouredine.hadjsaid}@g2elab.grenoble-inp.fr

ABSTRACT

Increased penetration of converter-interfaced primary energy sources to the electrical power system poses many different challenges to the design and operation of such systems. The intrinsic properties of these converter-interfaced units such as the lack of conventional inertia may jeopardize the system frequency stability specially in networks with mixed generation from conventional Synchronous Machines (SM). This article investigates the potential utilization of Virtual Inertia (VI) from the converter-based resources to mitigate such frequency stability issues in islanded distribution networks. Some recommendations for optimal dispatching and placement of VI devices are highlighted in the case study taking into consideration topological and different operating conditions.

I- INTRODUCTION

Climate change was initially the main driver for the integration of renewable energy resources into the electrical networks. Nevertheless, recent economic and geopolitical situation raised questions on energy security concerns. Experts think that the current situation demands integration of such units at a faster and much larger pace to decrease reliance on fossil fuel-based resources. However, economic and technical constraints to integrate such Inverter Based Resources (IBR) units and gradual retraction of conventional fossil fuel-based units remain open research topics [1].

At the present, power systems mostly utilize synchronous-based power generation units. These units are of large capacity and usually centralized and thus are more economic and provide huge intrinsic inertia reservoir [1]-[4]. On the other hand, many of the low-carbon technologies deployed are interfaced to the network through a power electronic converter. Such converters impose new challenges to the operation and design of the power systems, such as the small inertia related to these converter-based units, their intermittency and stability related issues [3], [5]. Frequency stability issue is the most obvious challenge in such low inertia networks. This is due to the fact that the power electronic converter interfacing such units and the grid masks their inertial response to any eventual unbalance [4].

Ongoing research on low-inertia power systems investigates such issues and Virtual Inertia (VI) appears as a promising solution especially in the context of networks with co-generation from conventional SM and IBR. Literature on the subject generally goes into one of two possible directions. The first starts from the fact that most inverters interfacing such IBR are controlled in a Grid-following (GFL) fashion and thus proposes different techniques to provide provisions of headroom in the generation by either operating the primary resource at a de-loaded operating point or allow for means of energy storage to provide the excess energy. VI can be dispatched using such techniques by measuring the rate of change of frequency and increasing the energy output—given enough energy is available from storage or by going back to nominal operating point—accordingly emulating an inertial effect [3], [6]-[7].

The second direction in literature studies the impact of emulating inertial behavior in the dynamics of Grid-forming (GFM) power converters. As we will investigate in detail later, inertial effect can be emulated in the frequency dynamics of the converter [8], [9]. However, headroom for excess power required is assumed to be available. This direction is the one investigated here by embedding such behavior in the frequency dynamics and analyzing the effect on the network frequency stability, i.e., maintaining the grid frequency and its rate of change (ROCOF) within acceptable bounds to prevent triggering of SM's protection relays [2].

The contribution of this article is thus threefold. First, techniques of embedding inertial response in the frequency dynamics of Grid-forming converter controllers and tuning criteria are presented. Second, investigation of the effect of VI on the operation of islanded distribution networks is carried out on a case study of the CIGRE MV distribution network benchmark [10] through a set of scenarios which takes into account different possible IBR penetration schemes and operating conditions. Third, some recommendations for optimal virtual inertia dispatching are extracted from the case study conducted and highlighted at the end.

II- EMBEDDING VI RESPONSE IN FREQUENCY DYNAMICS

The most simple and common grid-forming

synchronization technique is based on the conventional droop method, where synchronization between multiple parallel units is achieved from information about active power [8]. The most basic droop also known as static or zero order droop configuration is shown in Fig. 1-a. The idea behind droop is simple and actually inspired from the P-f and Q-V relations in SM, where frequency decreases as load active power increases and vice-versa, with similar relation between reactive power and terminal voltages.

However, since measurements' filter is required to achieve good attenuation of high frequency distortion components in the measured active power, a low-pass filter of cut-off frequency ω_f is added on the measured active power as shown in Fig. 1-b [11]. Since this filter dynamics only affect transients a derivative first order term appears in the frequency dynamics. This is the reason we call this configuration first order droop. Similarly, a second order droop configuration can be achieved by adding another low-pass filter with cut-off frequency ω_c as shown in Fig. 1-c.

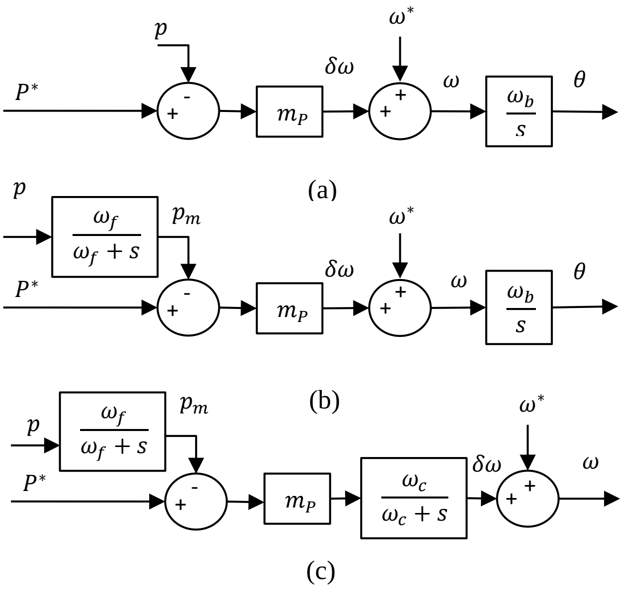

Figure 1: Different droop configurations for outer active power synchronization loop, (a) the zero-order droop, (b) the first order droop and (c) the second order droop configuration

In order to understand the logic about the second-order droop configuration, let us put the resulting dynamics of the different configurations in the canonical form summarized in Table I. A first conclusion deduced is that the steady state (s.s.) term (i.e., the steady state value of the frequency) is unaffected by the different configurations. On the other hand, only the transient dynamics are greatly affected. In case no filter is used, the dynamics are instantaneous and very abrupt as compared in Fig. 2. However, in the case of first and second order dynamics, an inertial behaviour is noticed. This could be explained by the analogy between the dynamics derived in Table I and the SM's swing dynamics:

$$2H.\frac{d\delta\omega}{dt} = P_m - P_e - D.\delta\omega \qquad (1)$$

where H is the SM inertia constant in seconds, $\delta\omega$ is the change in the electrical rotor angle in rad/s, P_m, P_e is the mechanical power input to the SM shaft and electrical power output respectively in per unit. D is the frictional damping in per unit.

By comparing (1) to the droop dynamics in Table I, and by identification we can deduce that the following terms are equivalent:

$$H_{eq}^{(2)} = \frac{\omega_c + \omega_f}{2m_p\omega_c\omega_f} \;\boldsymbol{or}\; H_{eq}^{(1)} = \frac{1}{2m_p\omega_f}, \qquad (2)$$

$$D_{eq} = \frac{1}{m_p} \qquad (3)$$

where $H_{eq}^{(1)}$ is the equivalent inertia constant of the 1st Order droop configuration while $H_{eq}^{(2)}$ is that of the 2nd Order configuration. m_p is the droop ratio in per unit. ω_c, ω_f are the filters cut-off frequencies in rad/s. D_{eq} is the equivalent virtual damping constant.

Table I: Frequency dynamics of different droop configurations proposed

	Transient Term			**S.S. Term**		
2nd Order	$\frac{1}{m_p\omega_c\omega_f}.\frac{d^2\delta\omega}{dt^2}$	$+\frac{\omega_c+\omega_f}{m_p\omega_c\omega_f}.\frac{d\delta\omega}{dt}$	$=$	P^*	$-p$	$-\frac{1}{m_p}\delta\omega$
1st Order		$\frac{1}{m_p\omega_f}.\frac{d\delta\omega}{dt}$	$=$	P^*	$-p$	$-\frac{1}{m_p}\delta\omega$
Zero Order		0	$=$	P^*	$-p$	$-\frac{1}{m_p}\delta\omega$

Thus, the advantage of using a second-order droop configuration is an additional degree of freedom to tune the equivalent inertia constant H_{eq} since the measurements' filter cut-off frequency ω_f choice should be low enough achieve good attenuation of high frequency distortion components as mentioned before as well as to avoid any interactions with inner control loops [11]. The droop ratio m_p cannot be altered freely as well because it affects the stability of the system [11]. Hence, ω_c provides an additional degree of freedom to tune the required equivalent inertia constant more freely. However, (2) can be reformulated as follows:

$$H_{eq}^{(2)} = H_{eq}^{(1)} + \frac{1}{2m_p\omega_c} \qquad (4)$$

In other words, if m_p and ω_f are pre-set and cannot be changed, a minimum equivalent inertia constant $H_{eq}^{(1)}$ is predefined. Thus, $H_{eq}^{(2)}$ is strictly larger than $H_{eq}^{(1)}$ and the equivalent inertia constant emulated can only be increased above that minimum $H_{eq}^{(1)}$.

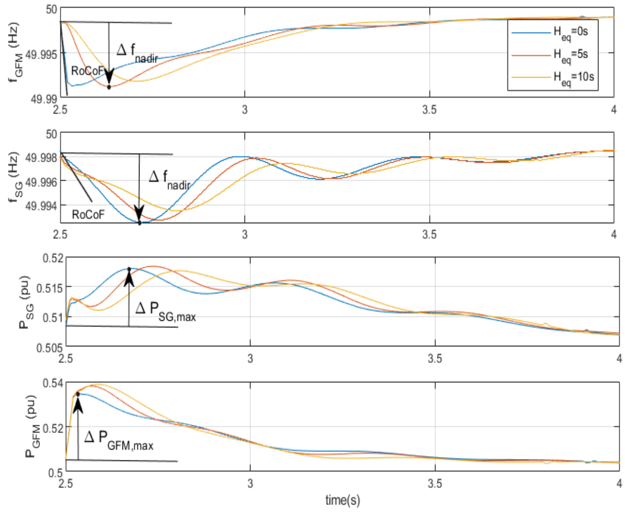

Figure 2: Comparison between zero order droop (blue) and second-order droop with H=5s (red) and H=10s (yellow) and different performance metrics introduced in Section III-C

III- CASE STUDY

As mentioned before, the objective of this article is to study the impact of the previously proposed VI configurations and dynamics on the operation and frequency stability of islanded distribution networks with different penetration levels of IBR and different operating conditions. In order to investigate that, we have adopted the CIGRE Medium Voltage Distribution Network Benchmark (European Configuration) [10] as the case study of our research objectives. This benchmark network is shown in Fig. 3 with the different PQ-loads shown on the table on the left.

A. Network Description

The CIGRE MV network benchmark [10] consists of 12 buses (0-11) and 11 constant PQ-loads with total consumed active and reactive power of 24.158 MW and 6.068 MVAr respectively. However, since we consider only the case of islanded networks operating as microgrids, the upstream network and bus 0 are removed (S1 is open). Three generation types are considered in this study. First conventional SM acting as generators are modelled and simulated. Second, PV generation connected through a Boost converter and a GFL-controlled inverter is considered and operated in Maximum Power Point Tracking (MPPT) mode. Third, generic GFM converter with VI embedded in the controls—as previously introduced in Section II—are also considered as a potential generation unit. The different scenarios of connecting these three sets of generation units and the different tests performed to emulate different operation conditions are detailed in the next subsection.

B. Scenarios & Tests Performed

In scenario (S1) only SM generation units are considered and connected to buses {1,4, and 8}. This scenario is the base scenario to which the following scenarios are compared to. Each SM is of 12 MW capacity, H=5s and droop coefficient=0.5%. PV units interfaced through GFL converters are considered starting from Scenario (S2) and maintained through all scenarios to study the effect of negligible inertia units on the operation of the network. It is always connected to bus {4} and of capacity 12 MW and operated in MPPT, thus its active and reactive power output depend on the references coming from the MPPT algorithm and user pre-set reactive power reference respectively. GFM converters with VI dynamics are considered in Scenarios (S3) and (S4). In S3, a GFM-VI

PQ-loads at each bus

P (MW)	Q (MVAr)
$P_1 = 19.839$	$Q_1 = 4.6371$
$P_2 = 0$	$Q_2 = 0$
$P_3 = 0.5017$	$Q_3 = 0.2089$
$P_4 = 0.4316$	$Q_4 = 0.1082$
$P_5 = 0.7275$	$Q_5 = 0.1823$
$P_6 = 0.5481$	$Q_6 = 0.1374$
$P_7 = 0.0765$	$Q_7 = 0.0474$
$P_8 = 0.5868$	$Q_8 = 0.1471$
$P_9 = 0.5737$	$Q_9 = 0.3556$
$P_{10} = 0.5433$	$Q_{10} = 0.1613$
$P_{11} = 0.3298$	$Q_{11} = 0.0827$
$\Sigma P = 24.158$	$\Sigma Q = 6.068$

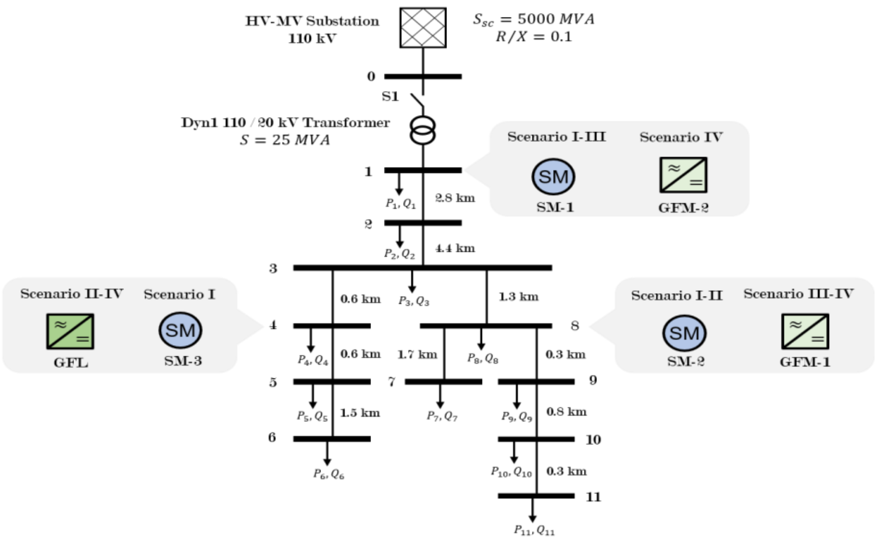

Figure 3: CIGRE European MV distribution network benchmark with the different PQ-loads at each bus and the different generation scenarios

replaces SM at bus {8}, its capacity is maintained at 12 MW with $H_{eq}^{(2)} = 5s$ and $m_p = 0.5\%$. Its emulated $H_{eq}^{(2)}$ is increased to $10s$ in S3'. In Scenario (S4) a 100% inverter-based islanded distribution network is tested by keeping the same configuration in S3 but replacing the last SM at bus {1} by a GFM-VI with the same ratings as the first GFM-VI deployed. In S4, GFM_1 at bus {8} emulates $H_{eq}^{(2)} = 5s$ while GFM_2 at bus {1} emulates $H_{eq}^{(2)} = 10s$ while in S4' their emulated $H_{eq}^{(2)}$ are swapped to study the effect of the location of VI placement on the inertia homogeneity in the grid. The different scenarios generation units' configurations are summarized in Fig. 3.

Three tests emulating different operating conditions are considered in this case study. The different scenarios (S1, S2, S3, S3', S4, S4') introduced above are subjected to the following disturbances:

i. Load step test: a +0.1 pu active power increase at all 11 PQ-loads is emulated.
ii. Single phase to ground short-circuit fault at bus {9} for 100ms.
iii. An irradiance decrease at the level of the PV at bus {4} by $-250\ W/m^2$.

C. Performance Metrics

To be able to compare the different scenarios to the base S1 scenario with conventional SM units and conventional synchronous inertia to the solutions proposed by the VI here by GFM converters, a set of performance metrics are selected to compare the performance after the different tests (i, ii, and iii) are introduced.

First, the frequency drop (also known as frequency nadir, c.f. Fig. 2) following the disturbances is an important metric, since higher frequency nadir can trigger load-shedding relays and cause un-intentional network splitting jeopardizing frequency stability. Second, since we are interested in protecting SM from high rate of change of frequencies, the SM machine connected at bus {1} frequency rate of change is measured and filtered through a low-pass filter to calculate the frequency RoCoF metric which is calculated as follows:

$$|RoCoF|_{max} = \max\left|\dot{f}_{node_1}\right| \quad (5)$$

In a similar manner to (4), the respective increase in active power following the disturbance (c.f. Fig. 2) by the different generating units at buses {1,4, and 8} are calculated also to quantify the control effort that the VI devices need to exert [9]. Only these three performance metrics will be thus considered to judge the effectiveness of the proposed solutions and network frequency stability compared to the base conventional network at S1.

IV- RESULTS & DISCUSSION

Comparing S2 where third of the generation is replaced by GFL-based PV generation with negligible inertia to S1, we can notice from Fig. 4, that the frequency RoCoF and nadir have considerably increased specially in case of a short-circuit fault (Test ii in orange). Additionally, due to maintaining of two-thirds of the generation as SM, the RoCoF and nadir are quite acceptable if compared to S3 in case of a single-phase short-circuit fault. That was also translated in the maximum injected active power after the fault as shown in Fig. 5. An increase in the injected active power by SM-1 and SM-2 can be spotted in S2 relative to S1 especially by the SM-2 since it is closer to the short-circuit fault.

The conclusion from this scenario is that a quite high penetration of negligible inertia units is possible, however increased RoCoF and nadir should be expected especially in case of high fluctuations of intermittent primary resource (e.g., irradiance or wind) and short-circuit faults, thus relay settings should be adjusted accordingly.

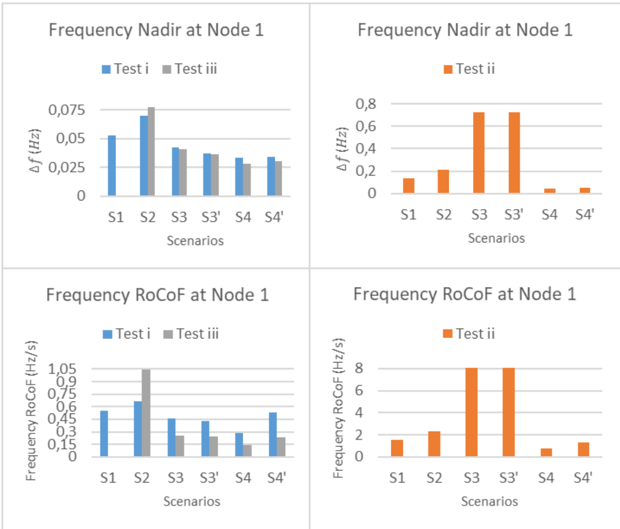

Figure 4: Frequency nadir and RoCoF metrics measured at bus {1}

A quite interesting highlight from S3 and S3' shows how the incorporation of GFM-VI devices in the generation mix increases the frequency stability and resilience of islanded distribution networks as can be deduced from RoCoF and nadir values in Fig. 4 compared to S1 and S2. Even more, the increased emulated inertia constant in S3' resulted in slightly better RoCoF and nadir. However, the respective increase in the injected active power by the GFM-VI device (GFM1 in Fig. 5) should be highlighted as a disadvantage of this approach. Another disadvantage can be seen in case of a short circuit fault (Test ii in orange). In this scenario where 66% approximately of the generation is supplied from converter-based generation with limited short-circuit capabilities, a short-circuit fault is very critical to the operation, stability and resilience of the network as can be seen from Fig. 4 and 5. Fault detection and clearance are crucial to the network safety.

Surprisingly enough, a short-circuit fault in a 100% converter-based generation with no SM (S4, S4'), resulted in lowest nadir and RoCoF values even compared to S1. Maximum injected active power is also very close to S1. This surprising result could be explained by the algorithms employed in the GFM-VI units and GFL controls to limit the currents during the faults (Transient Virtual Impedance technique). One can conclude from here that a network with mixed SM-IBR generation with high IBR penetration should be managed with much more caution than 100% IBR networks.

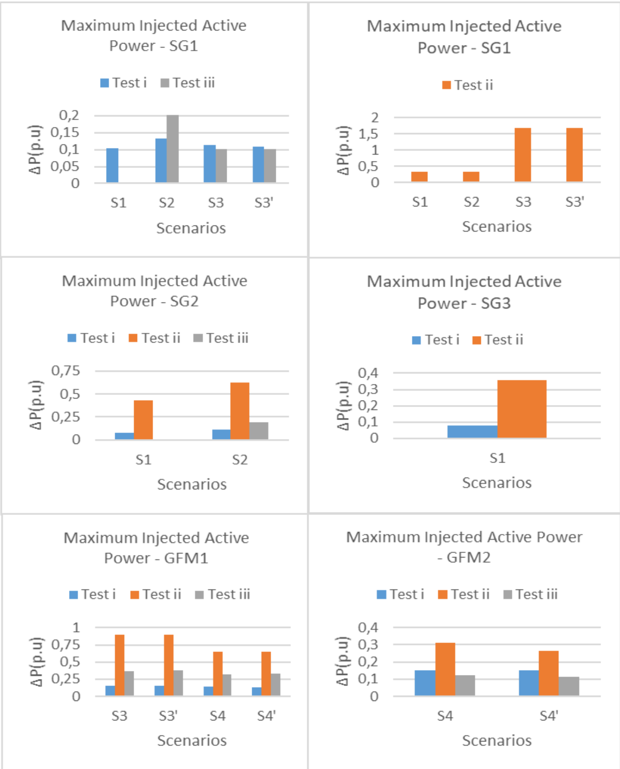

Figure 5: Maximum injected active power by the different units at buses {1,4, and 8} after the different disturbances (tests i, ii, and iii)

Additionally, an important highlight on the effect of geographical placement of VI can be extracted from comparing S4 to S4'. In S4, the inertia emulated at bus {8} is $H_{eq}^{(2)} = 5s$ while at bus {1} is $H_{eq}^{(2)} = 10s$ while in S4' that was swapped to study the effect of geographical placement of VI devices relative to the disturbance under study. A first conclusion is that the total amount of inertia is not the parameter to be optimized but actually where to place and dispatch the VI devices and their proximity to the disturbance, i.e., the inertia homogeneity across the network should be maintained [9], [12]. This could be concluded from Fig. 4 comparing S4' to S4 we can notice a slight increase in the value of the RoCoF post-fault. On the other hand, nadir was not impacted. However, it appears that type of the disturbance did not impact the RoCoF and nadir values but on the other hand it has great effect on the peak active power injected and thus the control effort that VI devices should exert.

V- CONCLUSIONS

Complexity of optimal placement of VI in the network taking into consideration different operating conditions and different possible geographical positions is illustrated and general recommendations and highlights based on the CIGRE MV distribution network benchmark as a case study are extracted. Most important highlights are the following: First, negligible inertia GFL devices require modifications to the protection relays of SM in case of high penetration especially in case of SC faults. Second, 100% IBR networks with GFM-VI devices can maintain the stability and resilience of islanded distribution networks and provide better performance to mixed SM-IBR networks with high IBR penetration. Third, optimal dispatching of GFM-VI units is a very complex problem which can be very different according to network topology, geographical placement of VI and SM units and operating conditions and faults to which the network is subjected to. However, the proposed VI embedded dynamics in the GFM converter controls can be easily dispatched and modified to provide optimal network operation in a wide variety of conditions.

VI- REFERENCES

[1] F. Milano, F. Dorfler, G. Hug, D. J. Hill, and G. Verbič, "Foundations and challenges of low-inertia systems" 2018.

[2] A. Ulbig, T. S. Borsche, and G. Andersson, "Impact of low rotational inertia on power system stability and operation," *IFAC Proc. Vol.*, vol. 19, pp. 7290–7297, 2014.

[3] K. S. Ratnam, K. Palanisamy, and G. Yang, "Future low-inertia power systems: Requirements, issues, and solutions - A review," *Renew. Sustain. Energy Rev.*, vol. 124, p. 109773, 2020.

[4] F. Kelada and J. Buire, "Contribution of Power Converters in Frequency Stability of Low-inertia Power Systems," Conférence des Jeunes Chercheurs en Génie Electrique, Croisic, France, 2022.

[5] J. Fang, H. Li, Y. Tang, and F. Blaabjerg, "On the Inertia of Future More-Electronics Power Systems," *IEEE J. Emerg. Sel. Top. Power Electron.*, vol. 7, no. 4, pp. 2130–2146, 2019.

[6] M. Dreidy, H. Mokhlis, and S. Mekhilef, "Inertia response and frequency control techniques for renewable energy sources: A review," *Renew. Sustain. Energy Rev.*, vol. 69, no. July 2016, pp. 144–155, 2017.

[7] Y. Z. Sun, Z. S. Zhang, G. J. Li, and J. Lin, "Review on frequency control of power systems with wind power penetration," POWERCON2010.

[8] R. Ofir, U. Markovic, P. Aristidou, and G. Hug, "Droop vs. virtual inertia: Comparison from the perspective of converter operation mode," *2018 IEEE Int. Energy Conf. ENERGYCON 2018*.

[9] B. K. Poolla, D. Groß, and F. Dörfler, "Placement and Implementation of Grid-Forming and Grid-Following Virtual Inertia and Fast Frequency Response," *IEEE Trans. Power Syst.*, vol. 34, no. 4, pp. 3035–3046, Jul. 2019.

[10] K. Strunz, C. Abbey, C. Andrieu, R. C. Campbell, and R. Fletcher, "Benchmark Systems for Network Integration of Renewable and Distributed Energy Resources," CIGRE Task Force C6.04.02, 2009.

[11] N. Pogaku, M. Prodanović, and T. C. Green, "Modeling, analysis and testing of autonomous operation of an inverter-based microgrid," *IEEE Trans. Power Electron.*, vol. 22, no. 2, pp. 613–625, Mar. 2007.

[12] A. Adrees, J. V. Milanović, and P. Mancarella, "Effect of inertia heterogeneity on frequency dynamics of low-inertia power systems," *IET Gener. Transm. Distrib.*, vol. 13, no. 14, pp. 2951–2958, 2019.